Effect of Fiber Variation on Staged Membrane Gas Separation Module Performance

B. Liu and G. G. Lipscomb
Chemical & Environmental Engineering, University of Toledo, Toledo, OH 43606

J. Jensvold
MG Generon, Pittsburg, CA 94565

The effect of fiber property variations on the performance of a two-stage system for gas separation was studied theoretically and experimentally. Variations in fiber inner diameter, slow gas permeance, or selectivity are considered. Variability in any of these properties is detrimental to performance, as characterized by product flow rate and product recovery (fraction of the feed recovered as a product). The performance decline increases as either property variation or product purity increase. The two-stage system can enhance performance significantly over a single sage. Permeate mixing is also beneficial to performance. Like a single stage, however, some fibers may stop producing a retentate product and consume product produced by other fibers for sufficiently large variation in size and permeance. The theory agrees well with experiments for the production of nitrogen from air.

Introduction

Industry is gradually embracing gas separation processes that utilize nonporous, polymeric membranes. These membranes are commonly produced in fine, hollow fiber form and combined together to form a module that is the mass-transfer equivalent of a shell-and-tube heat exchanger. The literature contains a vast body of work devoted to the development of membrane materials with better transport properties. Significantly less effort has been devoted to studies of module design and the factors that control, and ultimately limit, performance.

Of particular concern is the effect of nonuniform fiber properties, an inherent byproduct of real-world manufacturing processes, on performance. The literature discusses the effects of variable fiber inner diameter (ID) (Wickramainghe et al., 1985; Kruelen et al., 1993; Elmore and Lipscomb, 1995; Crowder and Cussler, 1997) and wall thickness (Crowder and Cussler, 1997) on performance for liquid separations. Significant reductions in performance can occur, especially at higher product purities. Three recent works discuss the effects of fiber size and transport properties on performance for gas separations. Rautenbach et al. (1998) predict large performance declines can result from variation in ID, dense skin thickness, or selectivity. Lemanski et al. (1999), and Lemanski and Lipscomb (2000) evaluate the effects of Gaussian variations in fiber ID, permeance, or selectivity on performance for both cross-flow and countercurrent modules used to produce nitrogen from air. They demonstrate that variation is detrimental to module performance. For a given percent variation, ID variation leads to the largest performance decline. As product purity increases, the performance decline increases. At the highest purities, fibers with the highest permeation to feed-rate-ratio may stop producing permeate and consume part of the product produced by other fibers; experimental measurements confirm this surprising conclusion. Lemanski et al. (1999) and Lemanski and Lipscomb (2000) also demonstrate that radial permeate mixing (that is, mixing in the direction normal to flow) mitigates the detrimental effects of property variation.

Here, we quantify the effect of variation in fiber ID, permeance, or selectivity on the performance of a two-stage system. For a given product composition, performance is characterized by the flow rate of the high-pressure retentate product leaving the system (R_s) and the ratio of this product flow rate to the feed flow rate to the system, the system recovery (θ_s), as illustrated in Figure 1. We extend the theoreti-

Correspondence concerning this article should be addressed to G. G. Lipscomb.

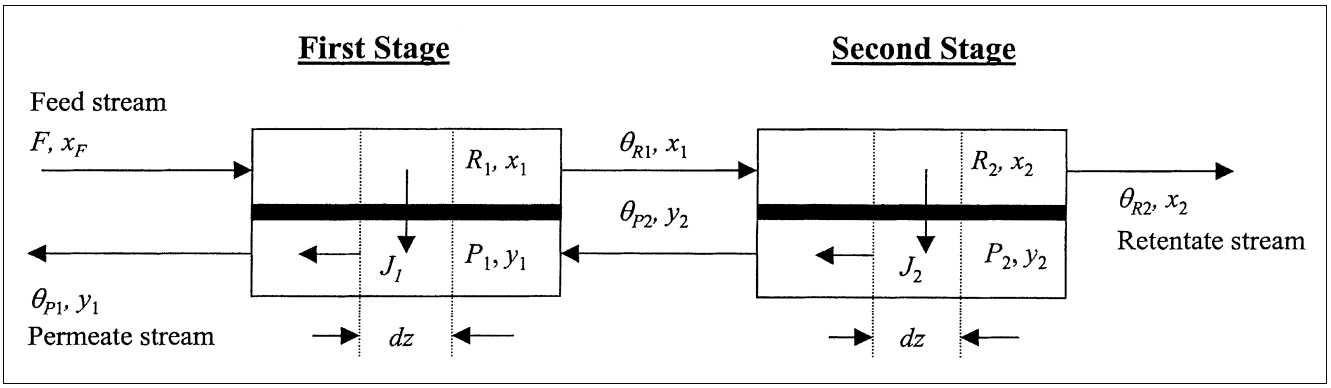

Figure 1. Two-stage system considered in this work.

Note that the product flow rate R_s is equal to R_2 and the product composition x_s is equal to x_2. The recovery for the entire system θ_s, is equal to R_2/F.

cal approach for simulating single stages described previously (Lemanski and Lipscomb, 2000) to two-stage cascades. Experimental measurements are in good agreement with theory for a model system. The results provide a basis for optimizing multistage cascades in the presence of fiber property variations.

One might expect staging to improve performance based on past simulations of staged systems (Lipscomb, 1996). However, previously reported improvements arise from the ability to recycle the permeate from one module to the feed of another: the permeate must be purer than the feed for this to be beneficial. *The staged configurations considered here would not result in any performance improvement in the absence of fiber property variations*. One might expect some enhancement in the presence of variations, because gas flowing through poorer performing fibers has a chance to move to better performing fibers between stages (retentate mixing between stages is beneficial like good radial permeate mixing). Of course, the converse is also true: gas flowing through better performing fibers has a chance to move to poorer performing fibers. This work demonstrates that the beneficial effects exceed the detrimental effects. Moreover, purity limitations of single modules can be overcome through staging. These observations are similar to those for past staging work, however, the underlying physics is fundamentally different: mixing the retentate in-between stages is responsible for the improvement instead of recycling a permeate stream of higher purity than the feed.

Analysis

Figure 1 illustrates the two-stage system considered. Two identical hollow fiber membrane modules are connected in series; each module is operated countercurrently. The retentate from the first stage is fed to the second stage while the permeate from the second stage is returned to the first stage and used as a permeate sweep. In the absence of fiber property variations, significant lumen or shell pressure drops and shell flow maldistribution, this two-stage system performs identically to a single stage. Although the analysis presented next assumes that the high-pressure retentate is the desired product (that is, nitrogen production from air), it could be readily extended to other cases.

One may envision other two-stage systems. However, the objective of this work is not to determine the optimum two-stage design but to evaluate the effects of variation on staged performance and the ability of the proposed theoretical analysis to predict performance. Once the analysis is validated, one can use it in optimization algorithms for staged systems (Qi and Henson, 1998).

The performance analysis is based on the following assumptions:

1. The feed contains two components and is an ideal gas.
2. The high-pressure stream is fed to the fiber lumens.
3. Lumen pressure changes are described by the Hagen-Poiseuille equation, and the magnitude of the lumen pressure drop is much smaller than the feed pressure.
4. Pressure changes negligibly within the shell.
5. Concentration polarization and axial diffusion are negligible.
6. Properties of a single fiber are independent of concentration and fiber length.
7. Operation is isothermal and steady state.
8. Module tubesheet thickness is small relative to the fiber length.

Given the above assumptions, mass and momentum balances on the lumen and shell for the jth fiber in stage i yield the following dimensionless performance equations:

$$\frac{d(x\theta_R)_{ij}}{dz_i} = -J_{ij}^A \tag{1}$$

$$\frac{d(\theta_R)_{ij}}{dz_i} = -J_{ij}^A - J_{ij}^B \tag{2}$$

$$\frac{d(y\theta_P)_{ij}}{dz_i} = \frac{d(x\theta_R)_{ij}}{dz_i} \tag{3}$$

$$\frac{d(\theta_P)_{ij}}{dz_i} = \frac{d(\theta_R)_{ij}}{dz_i} \tag{4}$$

$$\frac{d(\Pi_{ij})^2}{dz_i} = -N_{ij}^p(\theta_R)_{ij} \tag{5}$$

where z is the dimensionless axial distance (actual axial distance/module length), x is the fast gas (that is, more permeable component) composition in the high-pressure retentate, y is the fast gas composition in the low-pressure permeate, J is the dimensionless permeation rate per unit axial length, θ is the dimensionless flow rate (actual molar flow rate/feed molar flow rate), and Π is the dimensionless retentate pressure (actual pressure/feed pressure). The superscripts A and B denote the fast gas and slow gas, respectively, while the subscripts R and P denote the high-pressure retentate and low-pressure permeate, respectively. J_{ij}^A and J_{ij}^B are given by

$$J_{ij}^A = \alpha N_{ij}^h (x_{ij} - \gamma_{ij} y_{ij}) \tag{6}$$

$$J_{ij}^B = N_{ij}^h \left[(1 - x_{ij}) - \gamma_{ij} (1 - y_{ij}) \right] \tag{7}$$

where α is the ideal separation factor (ratio of fast gas permeance, Q^A to slow gas permeance Q^B) and γ is the dimensionless permeate to retentate pressure ratio (shell pressure/actual lumen pressure). Since we assume lumen pressure drops are much smaller than the feed pressure, γ_{ij} is approximately independent of z_i and $\gamma_{1j} = \gamma_{2j} = \gamma$. The dimensionless groups N^p and N^h are given by

$$N_{ij}^p = \frac{256 \mu R_g T L_i F_{ij}}{\pi (\mathrm{ID}_{ij})^4 p_f^2} \tag{8}$$

$$N_{ij}^h = \frac{\pi (\mathrm{OD}) L_i Q_{ij}^B p_f}{F_{ij}} = \frac{A_i Q_{ij}^B p_f}{F_{ij}} \tag{9}$$

where μ is the retentate viscosity, R_g is the ideal gas constant, T is the temperature, L is the total active fiber length, F is the fiber molar feed rate, ID is the fiber inside diameter, p_f is the feed pressure, and OD is the fiber outside diameter. Permeance (Q) is the ratio of the intrinsic, specific permeability to the effective membrane thickness based on the permeation area calculated using the fiber OD. Note that Eq. (9) can be used to compute F_{ij} for a given N_{ij}^h.

The boundary conditions for the first stage are:

$$\theta_{R1j}(z_1 = 0) = 1 \tag{10}$$

$$x_{1j}(z_1 = 0) = x_f \tag{11}$$

$$\Pi_1(z_1 = 0) = 1 \tag{12}$$

$$P_{1j}(z_1 = 1) = \overline{P_2}(z_2 = 0) \tag{13}$$

$$y_{1j}(z_1 = 1) = \overline{y_2}(z_2 = 0) \tag{14}$$

where x_f is the feed composition, $\overline{y_2}(z_2 = 0)$ is the mixing cup average fast-gas composition of the permeate from the second stage, and $\overline{P_2}(z_2 = 0)$ is the average permeate molar flow rate per fiber from the second stage (note that an overbar indicates an average value for all fibers in the bundle).

Boundary condition 10 states that the retentate flow rate in fiber j at the feed inlet is equal to the feed flow rate to that fiber. The composition and pressure of the retentate in fiber j at the feed inlet are set equal to the composition and pressure of the feed by boundary conditions 11 and 12, respectively. The permeate from the second module is used to sweep the first, so boundary condition 14 sets the composition of the permeate that enters the first module equal to the mixing cup average composition of the permeate that exits the second. Boundary condition 13 assumes the permeate from the second stage is distributed equally around each fiber in the first. The actual permeate flow would differ if significant shell side flow maldistribution exists. However, the prediction of flow distribution is a problem of equal magnitude to the one we consider here and the assumption of uniform distribution provides an upper bound on performance. The same assumption is the basis for virtually all past simulation work for module cascades (Lipscomb, 1996).

Boundary conditions for the second stage are given by

$$\theta_{R2j}(z_2 = 0) = 1 \tag{15}$$

$$x_{2j}(z_2 = 0) = \overline{x_1}(z_1 = 1) \tag{16}$$

$$\Pi_2(z_2 = 0) = 1 \tag{17}$$

$$\theta_{P2j}(z_2 = 1) = 0 \tag{18}$$

$$y_{2j}(z_2 = 1) = \frac{J_{2j}^A}{J_{2j}^A + J_{2j}^B} \tag{19}$$

where $\overline{x_1}(z_1 = 1)$ is the mixing cup average fast-gas composition from the first stage.

Boundary condition 15 stages that the retentate flow rate in fiber j at the feed inlet is equal to the feed flow rate to that fiber. Since the retentate product from the first module is the feed to the second, the composition and pressure of the retentate in fiber j at the feed inlet are set equal to the mixing cup average composition and pressure of the retentate that exits the first module by boundary conditions 16 and 17, respectively. The flow rate of the permeate is zero at the retentate exit, since a sweep is not used, as specified by boundary condition 18 while the composition is equal to the permeate composition produced in cross-flow (Lipscomb, 1996), as specified by boundary condition 19.

To solve these equations, one must specify fiber properties (OD, ID, L, α, Q^B), a fluid property (μ), operating conditions (T, p_f, γ), and a feed rate for each fiber in each stage (F). In actual operation, feed rates are not specified: the pressure drop across the system is specified instead. This makes the feed, or its dimensionless form N_{ij}^h, an additional variable that one must evaluate.

The two additional boundary conditions required to calculate F_{1j} and F_{2j} are

$$\Pi_1(z_1 = 1) = 1 - \Delta\Pi_1 \tag{20}$$

$$\Pi_2(z_2 = 1) = 1 - \Delta\Pi_2 \tag{21}$$

Since the overall system pressure drop is set, one cannot separate $\Delta\Pi_1$ and $\Delta\Pi_2$ without an additional constraint. This constraint is the requirement that the average feed flow rate

per fiber to the second stage ($\overline{F_2}$) must equal the average retentate flow-per-fiber from the first stage [$\overline{R_1}(z_1=1)$]

$$\overline{F_2}=\overline{R_1}(z_1=1) \tag{22}$$

Following Lemanski et al. (1999) and Lemanski and Lipscomb (2000), we will consider variations in ID, slow gas permeance, and ideal separation factor. A Gaussian distribution of each fiber property (the distribution is the same for each stage) is assumed

$$g(\phi)=\frac{1}{\sigma\sqrt{2\pi}}\exp\left(-\frac{(\phi-\overline{\phi})^2}{2\sigma^2}\right) \tag{23}$$

where ϕ is the value of the fiber property, σ is the standard deviation, and the overbar indicates the average value. The fraction of the fibers for which the property value falls in the interval $[\phi,\ \phi+d\phi]$ is equal to $g(\phi)d\phi$. The average value of some quantity ψ for all of the fibers in a bundle is given by

$$\overline{\psi}=\int_{\phi_{\min}}^{\phi_{\max}}\psi(\phi)g(\phi)d\phi \tag{24}$$

where $\psi(\phi)$ is the value of this quantity for fibers in which the variable material property has a value of ϕ, $\phi_{\max}$ the maximum value of the material property, $\phi_{\min}$ the minimum value, and the overbar indicates an average value. If more than one material property is variable, then one must evaluate a multiple integral over each of the properties. This work, however, considers only the variation of a single property at a time.

Equation 24 gives the average retentate flow rate from stage i as

$$\overline{R_i}(z_i=1)=\int_{\phi_{\min}}^{\phi_{\max}}F_i(\phi)\theta_{Ri}(\phi,1)g(\phi)d\phi \tag{25}$$

where $F_i(\phi)$ is the feed rate to fibers in stage i for which the variable material property takes on the value ϕ and $\theta_{Ri}(\phi,1)$ is the value of the dimensionless retentate flow rate for these same fibers at the retentate exit, $z_i=1$. The average retentate fast gas composition is given by

$$\overline{x_i}(z_i=1)=\frac{\int_{\phi_{\min}}^{\phi_{\max}}x_i(\phi,1)F_i(\phi)\theta_{Ri}(\phi,1)g(\phi)d\phi}{\overline{R_i}(z_i=1)} \tag{26}$$

where $x_i(\phi,1)$ is the retentate composition at the retentate exit for fibers in stage i for which the variable material property takes on the value ϕ. The numerator is the average retentate fast-gas flow rate.

Table 1. Typical Fiber Properties and Operating Conditions for Gas Separation Modules Designed to Produce Nitrogen from Air

OD	250 μm
ID	200 μm
L	1 m
Q^B	10^{-12} m^3(STP)/m$^2\cdot$s$\cdot$Pa
α	8
p_f	10^6 Pa

The average fast-gas composition of permeate from stage i is given by

$$\overline{y_i}(z_i=0)=\frac{\int_{\phi_{\min}}^{\phi_{\max}}y_i(\phi,0)F_i(\phi)\theta_{Pi}(\phi,0)g(\phi)d\phi}{\int_{\phi_{\min}}^{\phi_{\max}}F_i(\phi)\theta_{Pi}(\phi,0)g(\phi)d\phi} \tag{27}$$

where $y_i(\phi,0)$ is the composition at the permeate exit, $z_i=0$, of the permeate surrounding fibers in stage i for which the variable material property takes on the value ϕ, and $\theta_{Pi}(\phi,0)$ is the dimensionless permeate flow rate for these same fibers. The numerator is the average fast-gas permeate flow rate from the ith stage while the denominator is the average permeate flow rate $\overline{P_i}(z_i=0)$.

To determine the overall performance of the two-stage system, one must solve the corresponding performance equations for each fiber in each stage. The mass balances for individual fibers in each stage are linked by the permeate composition y, since all fibers contribute to the permeate. The value of y depends on the extent of radial mixing in-between fibers. Two limiting cases for mixing are considered here: no radial mixing and perfect radial mixing. One would expect the mixing that occurs in real modules to fall between these two limits. Order of magnitude estimates of diffusional fluxes in the gas phase and permeation rates across the membrane for current commercial modules (see Table 1 for typical fiber properties and operating conditions) suggest concentration variations in the gas phase are less than 1% over length scales equivalent to approximately one-hundred fiber diameters.

For the no mixing case, each fiber in each bundle performs independently and no additional performance equations are needed to predict bundle performance. For the perfect mixing case, the permeate from all fibers in each bundle is well mixed; therefore, for a given axial position, the permeate composition is the same for all fibers: $y_i(\phi,z_i)=\overline{y_i}(z_i)$. Equation 14 is still used to calculate $\overline{y_1}(z_1=1)$ while $\overline{y_2}(z_2=1)$ is given by

$$\overline{y_2}(z_2=1)=\frac{\int_{\phi_{\min}}^{\phi_{\max}}J_2^A(\phi,1)F_2(\phi)g(\phi)d\phi}{\int_{\phi_{\min}}^{\phi_{\max}}\left[J_2^A(\phi,1)+J_2^B(\phi,1)\right]F_2(\phi)g(\phi)d\phi} \tag{28}$$

instead of Eq. 19. Note that $J_2(\phi,1)$ is the permeation rate across the membrane at the retentate exit ($z_2 = 1$) for fibers in the second stage for which the variable material property takes on the value ϕ, and the superscripts A and B refer to the permeation rates of the faster and slower permeating species, respectively.

Overall bundle performance is quantified by calculating the mixing cup average composition, recovery, and flow rate of the product from the system. Here, we assume the retentate produced by the second stage is the desired product as is the case for nitrogen production from air. The product mixing cup average composition $\bar{x}_s$ and flow rate $\bar{R}_s$ are given by Eqs. 26 and 25, respectively, by setting $i = 2$ (the subscript s denotes the product of the system). The average retentate recovery for the system is given by

$$\bar{\theta}_s = \frac{\overline{R_2}(z_2 = 1)}{\int_{\phi_{\min}}^{\phi_{\max}} F_1(\phi) g(\phi) d\phi} \tag{29}$$

where the denominator is the average feed flow rate entering the first stage. Since the feed to the first stage is the stream that requires compression, this definition of recovery reflects the fraction of the compressed gas that is recovered as product.

The performance equations for each stage correspond to split boundary value problems. We use the finite difference method to obtain a numerical approximation to their solution. Derivatives are approximated by second-order differences except at $z_i = 0$ and $z_i = 1$ where a first-order difference is used. The resultant set of nonlinear algebraic equations is solved using a Newton-Raphson algorithm for the unknown values of θ_{Rij}, θ_{Pij}, Π_{ij}, x_{ij}, and y_{ij} at each node and F_{ij} for each stage. A grid refinement analysis is performed to evaluate numerical error.

The performance equations for each stage are linked by the requirements that the retentate flow from the first stage must equal the feed flow to the second and the permeate flow from the second is used as a sweep in the first. To solve these coupled equations, we guess values for $\overline{P_2}(z_2 = 0)$ and $\overline{y_2}(z_2 = 0)$ and calculate $\overline{R_1}(z_1 = 1)$ and $\overline{x_1}(z_1 = 1)$ from the performance equations for the first stage. Then, the second-stage equations are solved to obtain calculated values for $\overline{P_2}(z_2 = 0)$ and $\overline{y_2}(z_2 = 0)$. If the calculated and guessed values are sufficiently close, the calculation is stopped. Otherwise, the values of $\overline{P_2}(z_2 = 0)$ and $\overline{y_2}(z_2 = 0)$ are updated and the calculation repeated. The Nelder-Mead simplex search algorithm, implemented in MATLAB (The MathWorks Inc.) as the function FMINS, is used to perform this minimization.

Equations 25–29 are evaluated using Gauss-Hermite quadrature (Carnahan et al., 1990). This method was developed especially for integrands including a factor of e^{-x^2} and

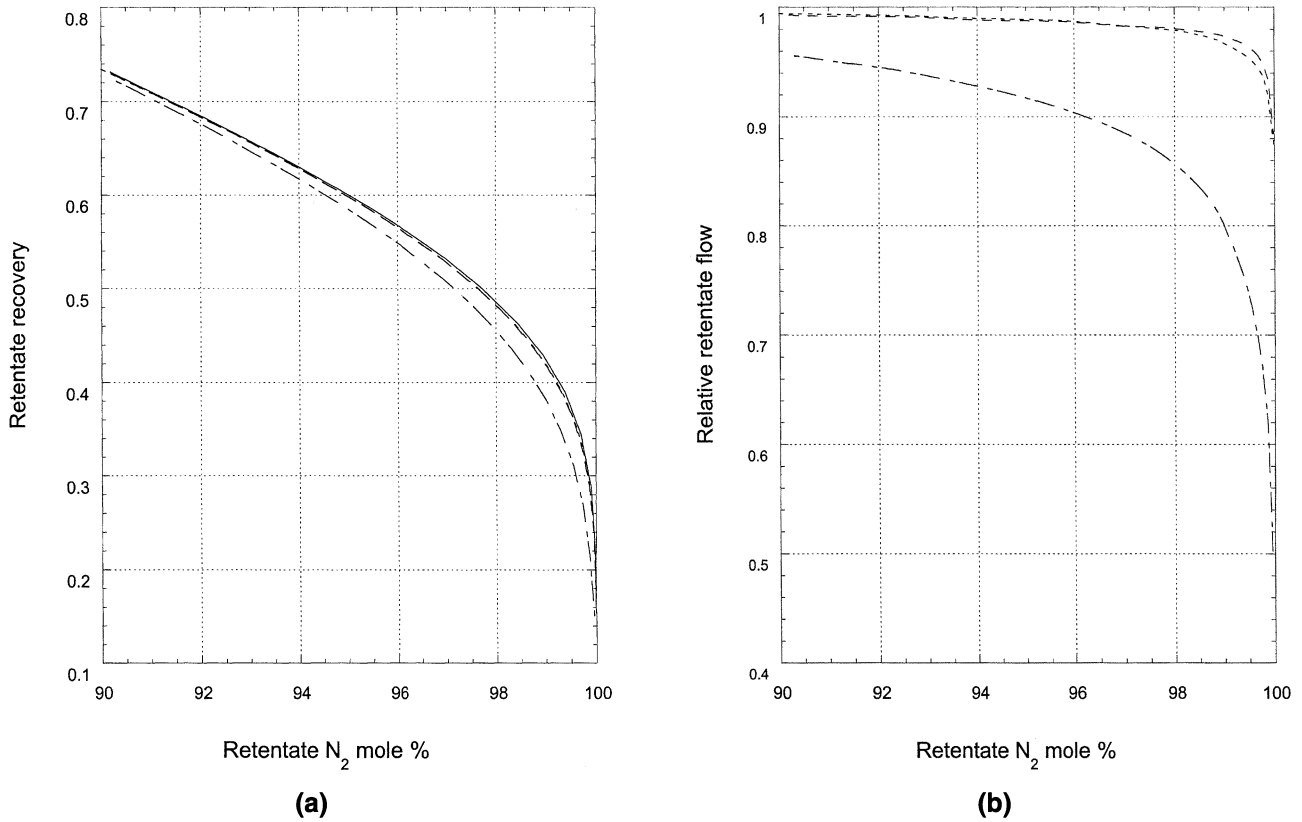

Figure 2. Effect of variation in ID, Q^B and α on performance with no permeate mixing.

(a) Retentate recovery as a function of product N_2 mol fraction; (b) relative retentate flow rate as a function of product N_2 mol fraction. The lines in both figures are: solid line, no variation; long dash, 15% α variation; short dash, 15% Q^B variation; dot-dash, 10% ID variation.

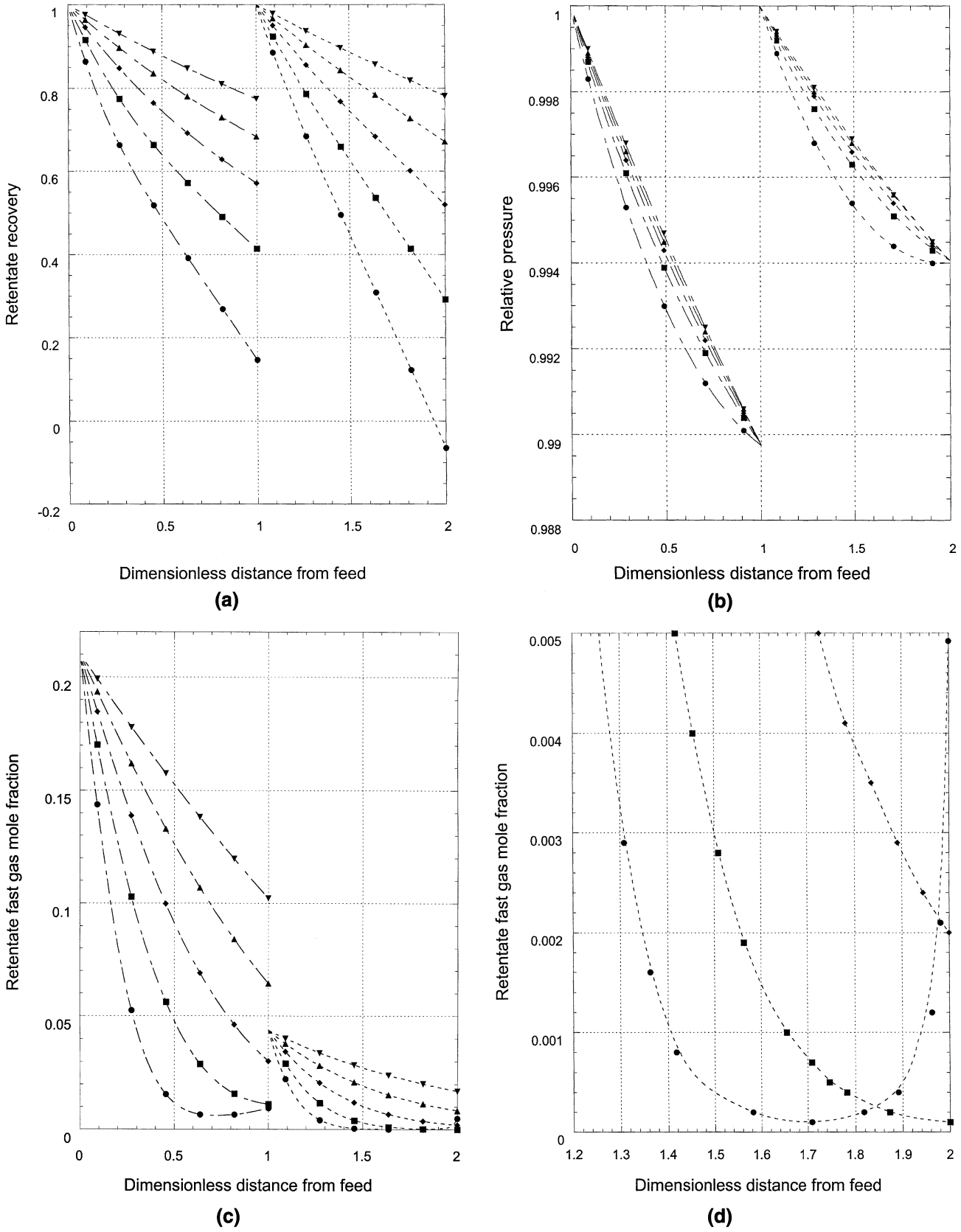

Figure 3. Separate fiber profiles for a two-stage system with 10% ID variation and no permeate mixing producing a product with 99.5% nitrogen.

(a) Retentate recovery; (b) retentate pressure; (c) retentate fast gas mol fraction, and (d) retentate fast gas mol fraction near product end of second stage. The lines in all figures are: dot-dash, first stage; short dash, second stage. The markers are: ● $ID/\overline{ID} = 0.71$; ■ $ID/\overline{ID} = 0.86$; ◆ $ID/\overline{ID} = 1$; ▲ $ID/\overline{ID} = 1.14$; ▼ $ID/\overline{ID} = 1.29$.

converts the integrals to finite sums. For example, Eq. 25 for $\overline{R_2}(z_2 = 1)$ is approximated using

$$\overline{R_2}(z_2 = 1) = \frac{1}{\sqrt{\pi}} \sum_{k=1}^{n} w_k \theta_{R2}(\phi_k, 1) F_2(\phi_k) \qquad (30)$$

where n is the number of quadrature points, the subscript k indicates the value evaluated at a specific quadrature point (that is, a particular value of ϕ), and w_k are the weight factors. Values for ϕ_k and w_k are tabulated as a function of n. Increasing n improves the accuracy of the approximation.

The integration limits must be extended to $\pm\infty$ to use the Gauss-Hermite quadrature. This approximation has been adopted in past studies of fiber property variation (Lemanski et al., 1999; Lemanski and Lipscomb, 2000), and it is expected to have little effect on the results for sufficiently small σ. Moreover, assigning values for the difficult to determine limits $\phi_{\min}$ and $\phi_{\max}$ is avoided.

Results

To simulate the performance of current commercial nitrogen systems, we set $\bar{\alpha} = 8$ and $\gamma = 0.1$ (see Table 1 for typical fiber properties and operating conditions). Five quadrature points and 56 spatial nodes were used for all simulations based on a mesh refinement analysis. Increasing the number of quadrature points from 3 to 5 and the number of nodes from 28 to 56 gives values for $\overline{R_s}$ and $\bar{\theta}_s$ that differ by less than 1% over the entire $\bar{x}_s$ range considered.

The discussion that follows refers to percent variation and relative retentate flow. *Percent variation* is the ratio of the standard deviation to the mean value of a property expressed as a percentage ($\sigma/\overline{\phi} \times 100\%$), while *relative retentate flow* is the ratio of the product retentate flow rate from a module with a variable fiber property to the flow from a module with no variation [$\overline{R}_S(\sigma)/\overline{R}_S(\sigma = 0)$]. The values of relative retentate flow and recovery $\bar{\theta}_s$, as a function of product purity $\bar{x}_s$, completely characterize module performance. Design changes that increase relative flow or recovery are said to improve performance.

Figure 2 compares the effects of comparable variations in ID, Q^B, and α on performance for the no mixing case. The variation in ID is less than that in Q^B and α, because, for a 15% variation, retentate recoveries were negative over the entire retentate composition range for the quadrature point corresponding to the smallest ID fibers ($\mathrm{ID}/\overline{\mathrm{ID}} = 0.57$) in the second stage. We discuss the implications of this later. To the best of our knowledge, the percent variations used in Figure 2 and subsequent figures are representative of the ranges of values found industrially.

The predicted performance decline for 15% variation in Q^B and α is much smaller than for a 10% ID variation. For

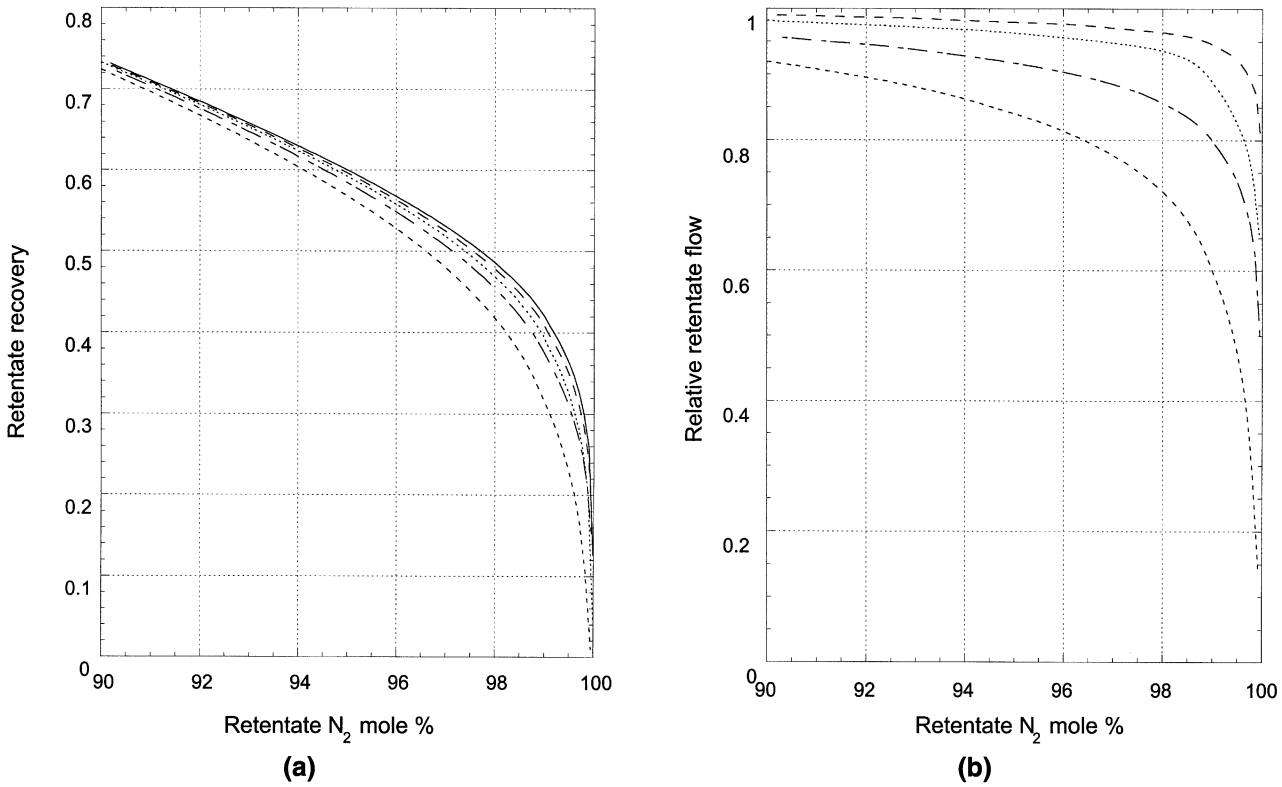

Figure 4. Effect of variation in ID and module staging on performance with no mixing.

(a) Retentate recovery as a function of product N_2 mol fraction; (b) relative retentate flow rate as a function of product N_2 mol fraction. The lines in both figures are: solid line, no variation; long dash, 5% ID variation/two-stage; dot, 5% ID variation/single-stage; dot-dash, 10% ID variation/two-stage; short dash, 10% ID variation/single stage.

example, at $\bar{x}_s = 0.005$ (99.5% nitrogen), both $\overline{\theta_s}$ and $\overline{R_s}$ decrease by less than 5% for a 15% Q^B or α variation, while $\overline{\theta_s}$ and $\overline{R_s}$ decrease by 16% and 26%, respectively, for a 10% ID variation.

The observation that ID variations have the greatest effect on performance is consistent with the results of Lemanski and Lipscomb (2000) for a single stage. Since fiber flow rate is proportional to ID^4, a 10% change in fiber ID leads to a 46% change in flow rate. Consequently, gas flows in smaller fibers will be lower than in larger fibers and smaller fibers will produce a higher purity retentate at lower recovery than larger fibers.

The negative retentate recoveries predicted for 15% ID variation are consistent with the hypothesis that the feed to some fibers may completely permeate from the lumen to the shell. At the point of complete permeation, the retentate flow drops to zero, and one cannot integrate the lumen mass balances (Eqs. 1 and 2) beyond this point. Physically, this implies that some of the retentate from fibers that produce a product must enter the fibers in which complete permeation occurs at the product end $z_i = 1$. This backflow completely permeates as well, and the point of complete permeation for the gas entering at $z_i = 1$ must coincide with the point of complete permeation for the gas entering at $z_i = 0$. To simulate this behavior, we follow the approach of Lemanski and Lipscomb (2000) and replace the component mass balance (Eq. 1) at $z_i = 1$ with the boundary condition that the retentate composition is equal to the mixing cup average composition of the product from producing fibers $\bar{x}_i$ calculated using Eq. 26. The point of complete permeation and the pressure there are set by the requirements that the retentate flows from $z_i = 0$ and $z_i = 1$ must vanish and the composition of the gas in both flows must be equal.

Figure 3 illustrates the changes in retentate recovery, pressure, and composition that occur with axial distance for fibers that correspond to each of the five quadrature points in each stage. In this figure, values of distance less than 1 correspond to the first stage, while the values between 1 and 2 correspond to the second (that is, 1 is added to z_2). The profiles shown are for a two-stage system with 10% ID variation and no permeate mixing producing a 99.5% nitrogen product.

Figure 3a illustrates how retentate recovery varies with axial distance. Positive values indicate a flow from the feed to the product end, while negative values indicate a flow in the opposite direction. Since the permeate always flows from the product to the feed end, fibers operate in a countercurrent mode when recoveries are positive, but operate in a cocurrent mode when recoveries are negative. The point of zero retentate flow, where the retentate has completely permeated, corresponds to $\theta_R = 0$. Figure 3 indicates complete permeation occurs in only one fiber, the smallest fiber ($ID/\overline{ID} = 0.71$) in the second stage, at $z = 1.94$.

Figure 3b illustrates the variation of retentate pressure with axial distance. For each fiber in the first stage and the four

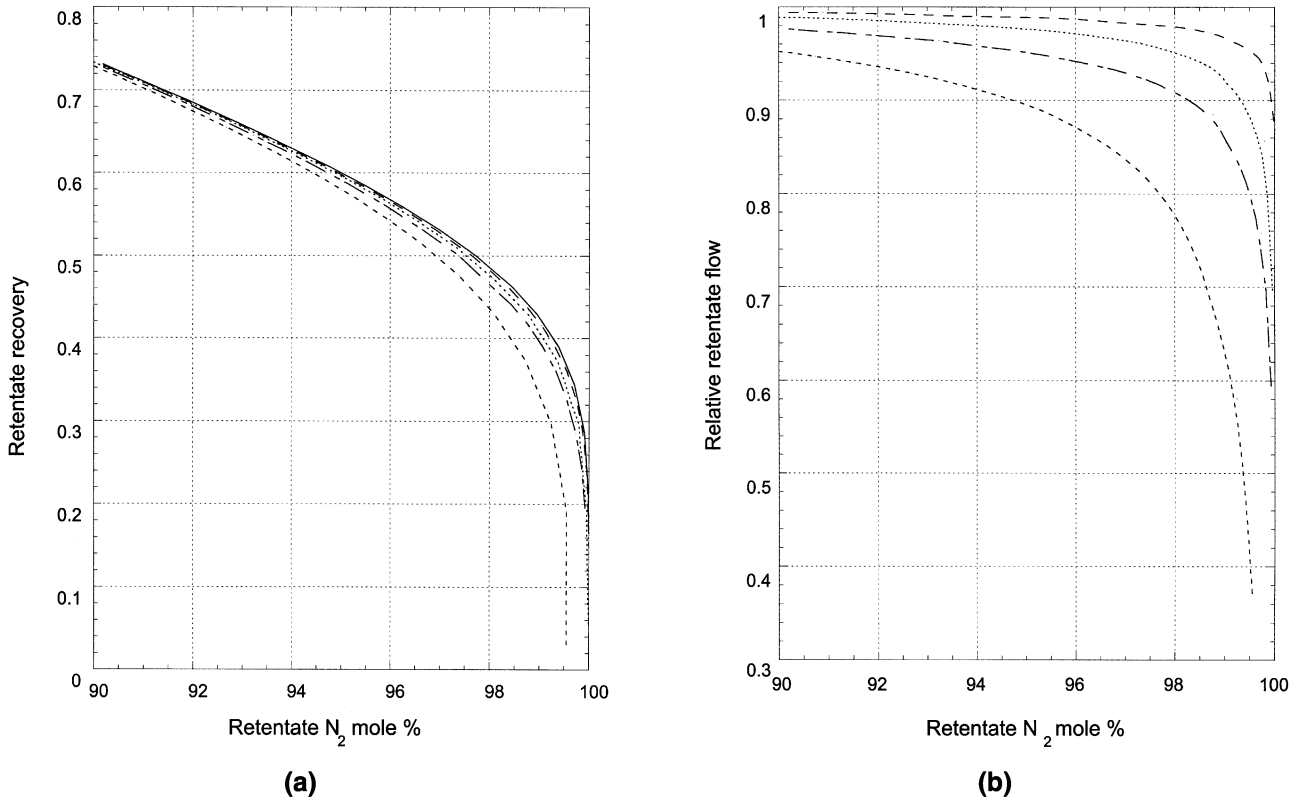

Figure 5. Effect of variation in Q^B and module staging on performance with no mixing.

(a) Retentate recovery as a function of product N_2 mol fraction; (b) relative retentate flow rate as a function of product N_2 mol fraction. The lines in both figures are: solid line, no variation; long dash, 15% Q^B variation/two-stage; dot, 15% Q^B variation/single-stage; dot-dash, 30% Q^B variation/two-stage; short dash, 30% Q^B variation/single-stage.

largest fibers in the second, pressure decreases monotonically from inlet to outlet. However, for the smallest fiber in the second stage, the pressure passes through a minimum at the point where $\theta_R = 0$ and then increases to the outlet pressure. The presence of a minimum is required for flow to occur from both ends of the fiber.

Figure 3c illustrates the variation of retentate fast gas composition with axial distance. Like pressure, fast gas composition decreases monotonically with axial distance for all fibers except the smallest fiber. The composition passes through two minimum values, one in each stage, $z = 0.70$ and $z = 1.7$, respectively. The region around $z = 1.7$ is magnified in Figure 3d.

This behavior arises from the nature of the permeate sweep in each stage. In the second stage, the product retentate that enters the smallest fiber and flows toward the feed end completely permeates as the gas flows from $z = 2$ to $z = 1.94$. This produces a permeate sweep around the smallest fiber that possesses the same composition as the retentate product. The sweep increases the oxygen composition of the permeate for $z < 1.94$ in the second stage and reduces the oxygen partial pressure driving force for permeation. The reduction is large enough that the oxygen composition of the retentate increases as it flows from $z = 1.7$ to 1.94, the point of complete permeation. Note that oxygen and nitrogen always permeate from the high-pressure retentate to the low-pressure permeate, but the ratio is lower than one would expect based on performance predictions for modules without fiber variation. Similar behavior occurs in the first stage where the permeate from the second stage is distributed around each fiber in the first. The ratio of oxygen to nitrogen permeation is reduced by the permeate sweep from the second stage and leads to an increase in retentate composition as the retentate flows from $z = 0.7$ to 1.0 in the smallest fiber.

Figure 4 illustrates the effect of ID variation and module staging on module performance for the no permeate mixing case. The performance of the two-stage system is significantly better that that of a single stage with 10% ID variation over the entire product purity range shown. For example, at 99.5% nitrogen, retentate recovery and flow rate decrease by 16% and 26%, respectively, for the two-stage system and by 35% and 50%, respectively, for the single stage. For both single and two-stage systems, performance decreases as variation increases.

Why does module staging improve performance? Figure 4 indicates that the decrease in performance due to property variation increases dramatically as product recovery decreases (that is, product purity increases). Therefore, operating a module at higher recoveries reduces the detrimental effects of property variation. In a staged system, both stages are operated at higher recoveries than a single stage, so one would expect less drop in performance in each stage. The cumulative drop for the system is also lower because of the strong, nonlinear dependence of performance on recovery.

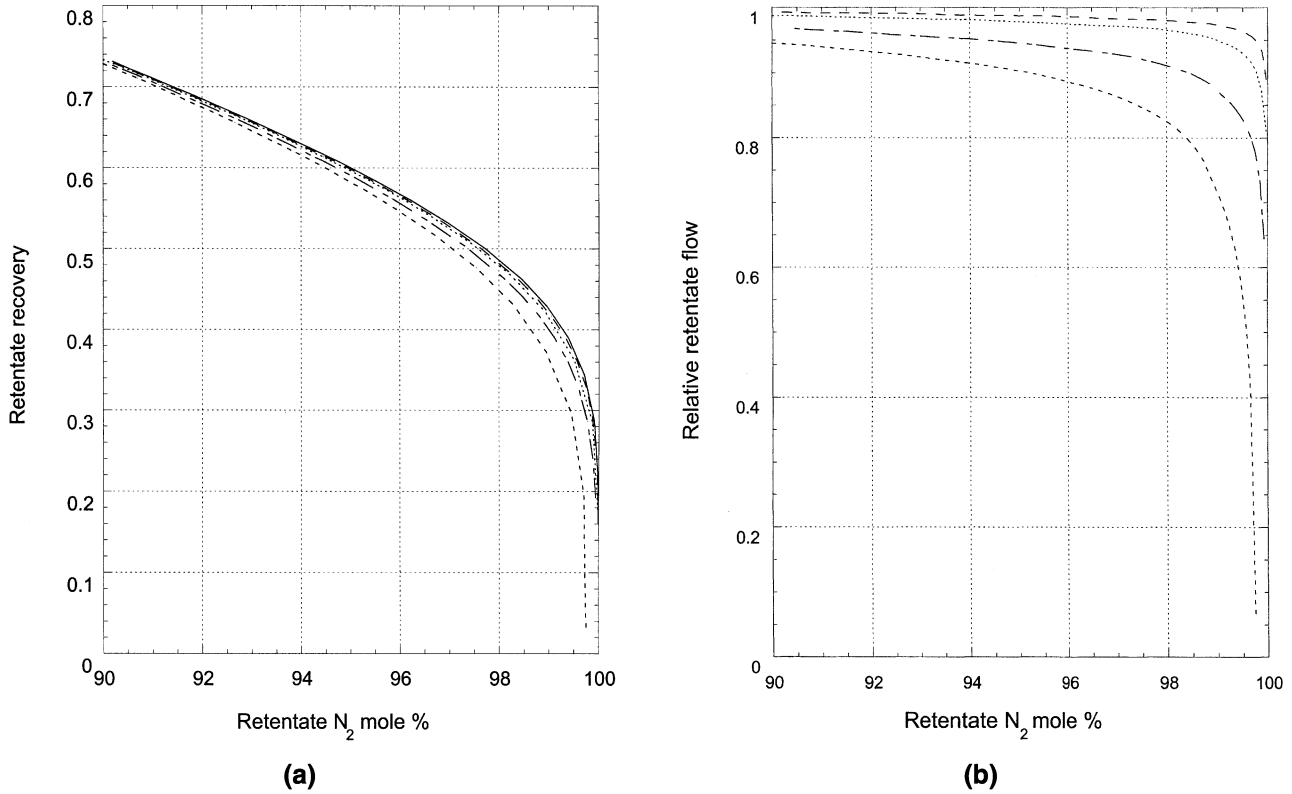

Figure 6. Effect of variation in α and module staging on performance with no mixing.

(a) Retentate recovery as a function of product N_2 mol fraction; (b) relative retentate flow rate as a function of product N_2 mol fraction. The lines in both figures are: solid line, no variation; long dash, 15% α variation/two-stage; dot, 15% α variation/single-stage; dot-dash, 30% α variation/two-stage; short dash, 30% α variation/single-stage.

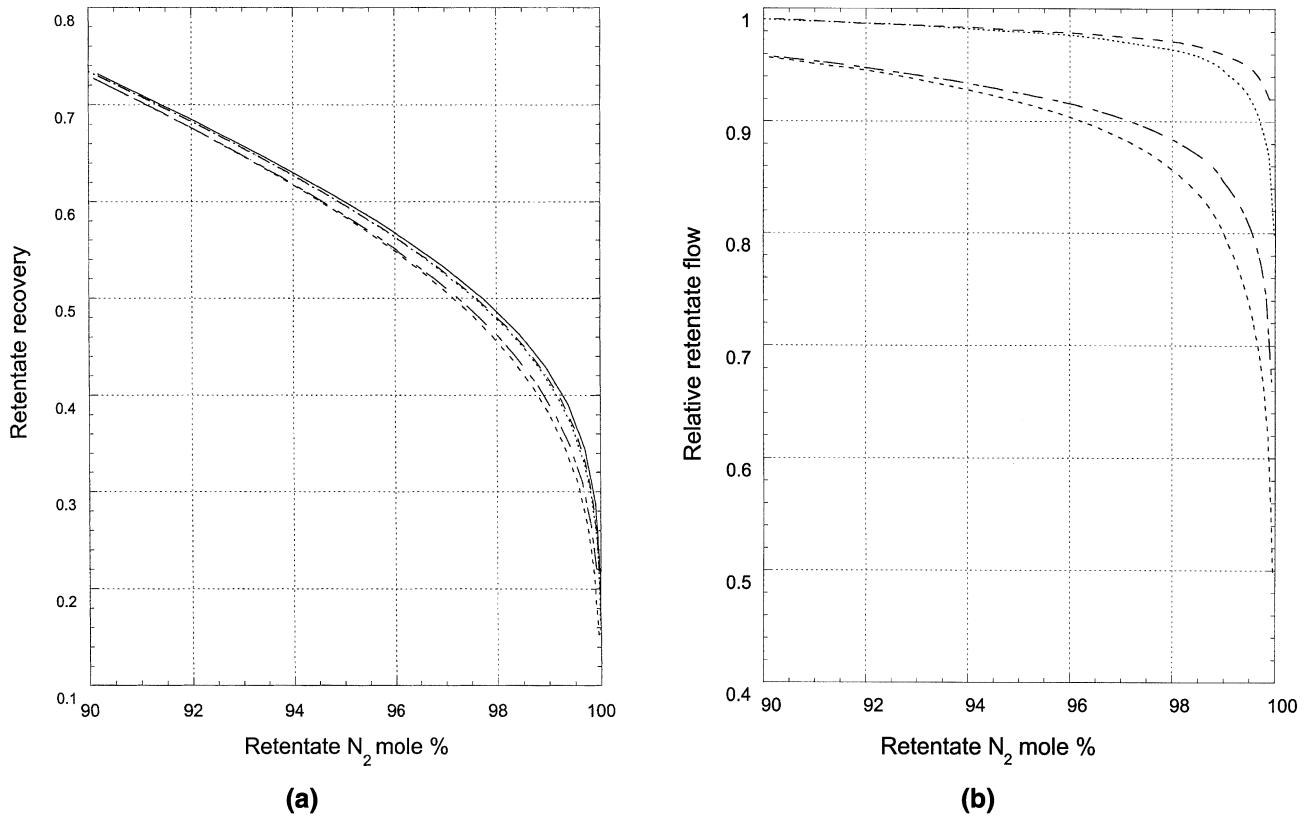

Figure 7. Effect of variation in ID variation and permeate mixing on performance.

(a) Retentate recovery as a function of product N_2 mol fraction; (b) relative retentate flow rate as a function of product N_2 mol fraction. The lines in both figures are: solid line, no variation; long dash, 5% ID variation/permeate mixing; dot, 5% ID variation/no mixing; dot-dash, 10% ID variation/permeate mixing; short dash, 10% ID variation/no mixing.

One might also rationalize the beneficial effect of staging by noting that staging allows gas flowing in poorer performing fibers an opportunity to move to better performing fibers in between stages. Although the converse is also true (that is, gas flowing in better performing fibers can move to poorer performing fibers), the increase in performance is larger than the decrease, so the net effect is a performance improvement.

Use of three or more stages may further improve performance. The performance enhancement may not be as significant, though, since pressure drops due to increased flows and flow-path length will reduce the partial pressure driving force for permeation.

Figure 5 illustrates the effects of variation in Q^B and module staging on performance for the no permeate mixing case. Qualitatively, the performance changes are similar to those observed for ID variation. As permeance variation increases, performance decreases. Additionally, staging improves performance. For example, at 99.5% nitrogen, a 30% permeance variation decreases recovery and flow rate by 40% and 60%, respectively, for a single stage compared to 11% and 19%, respectively, for a two-stage system. Interestingly, at 99.5% nitrogen, the fibers with $Q^B/\overline{Q^B} = 1.86$ stop producing product in a single stage, while no fibers stop producing product in a two-stage system. This further illustrates the beneficial effect of staging.

Figure 6 illustrates the effects of α variation and module staging on performance for the no permeate mixing case. Similar to ID and Q^B variation, performance decreases as the percent variation increases and staging improves performance. For example, at 99.5% nitrogen, a 30% α variation decreases recovery and flow rate by 25% and 40%, respectively, for a single stage compared to 9% and 16%, respectively, for a two-stage system. In contrast to the ID and Q^B variations, we did not observe complete permeation in any of the cases simulated. This is consistent with prior work for single stages (Lemanski and Lipscomb, 2000).

Figure 7 illustrates the effect of percent variation in ID and permeate mixing on the performance of a two-stage system. Like one-stage systems, permeate mixing improves performance. For 99.5% nitrogen, a 10% ID variation decreases recovery and flow rate by 11% and 18%, respectively, for a two-stage system with mixing, compared to 16% and 26%, respectively, with no mixing.

Results are not shown for the effects of permeate mixing on performance for Q^B and α variation, but the results are similar to those for a single stage (Lemanski and Lipscomb, 2000). Permeate mixing improves performance for Q^B variations and has a negligible effect on performance for α variation. The qualitative effects of fiber property variation and permeate mixing on performance predictions are summarized in Table 2.

Table 2. Qualitative Effects of Fiber Property Variations on Module Performance

Property	Performance Change Relative to Module with No Property Variation	Sensitivity to Permeate Mixing
ID	Large	Moderate
Q^B	Moderate	Moderate
α	Moderate	None

Experimental Studies

The experimental two-stage system shown in Figure 8 is used to validate the theoretical analysis. The system consists of two identical commercial modules (Permea, Inc., Model PPA-22AD) connected in series. Compressed air (from a laboratory supply line) is lumen-fed to the first stage. The permeate from the first stage is vented to the room, while the reject is lumen-fed to the second stage. The permeate from the second stage is used to sweep the first. In the absence of fiber property variation, past simulations of staged configurations would predict no performance enhancement due to staging for this configuration. To avoid the need to characterize the variation in fiber properties for each module, a low-permeance polypropylene tube is placed parallel with each module. The tube shares a common inlet and outlet with the module and simulates the effect of a number of zero permeance fibers. The large difference in permeance between the fibers in the module and the tube allows us to neglect property variation for fibers in the module; the effect of any variation is small relative to the effect of the bypass tube.

A needle valve is present at the end of each bypass tube to control the fraction of the total feed that enters the tube. Varying the position of the valve corresponds to varying the number of low permeance fibers. All of the data reported here are for a single valve position. At this position, approximately 10% of the total feed enters the tube.

To evaluate system performance, flow rate, composition and pressure are measured at the locations illustrated in Figure 8. System performance is characterized by computing the overall retentate recovery as a function of retentate composition. In the experiments, $p_f = 85$ psig and $\gamma = 0.147$. Mass balances for each experimental run closed to within 5% or less.

To simulate performance, a discrete distribution of fiber properties is used instead of a continuous Gaussian variation. All of the fibers in each module are assigned average values for ID, Q^B, and α while the fibers associated with the bypass tube are assigned zero permeance. Average property values were chosen that minimized the difference between predicted and experimental recoveries for nitrogen production from air for each module operated without the bypass tube. Theoretical results for the well-mixed permeate and no mixing cases are identical for this type of fiber distribution because the zero permeance fibers do not produce permeate. Mixing the permeate from the two types of fiber (the fiber in the module and the fiber represented by the bypass tube) does not change the permeate composition since no permeate is produced by one of the fiber types.

Figure 9 illustrates the variation of retentate recovery with composition for each module without the bypass tube. The predicted recovery, using best fit average material properties,

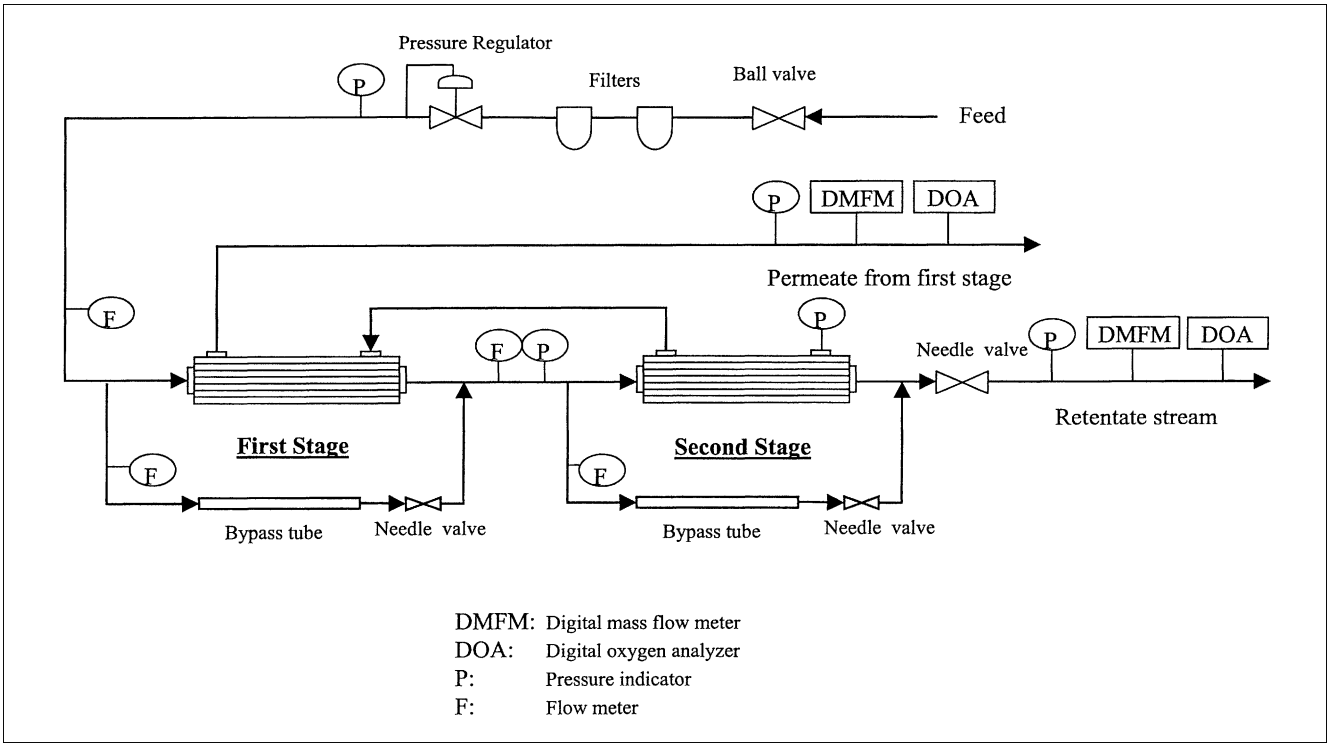

Figure 8. Experimental apparatus for a two-stage system with fiber variations.

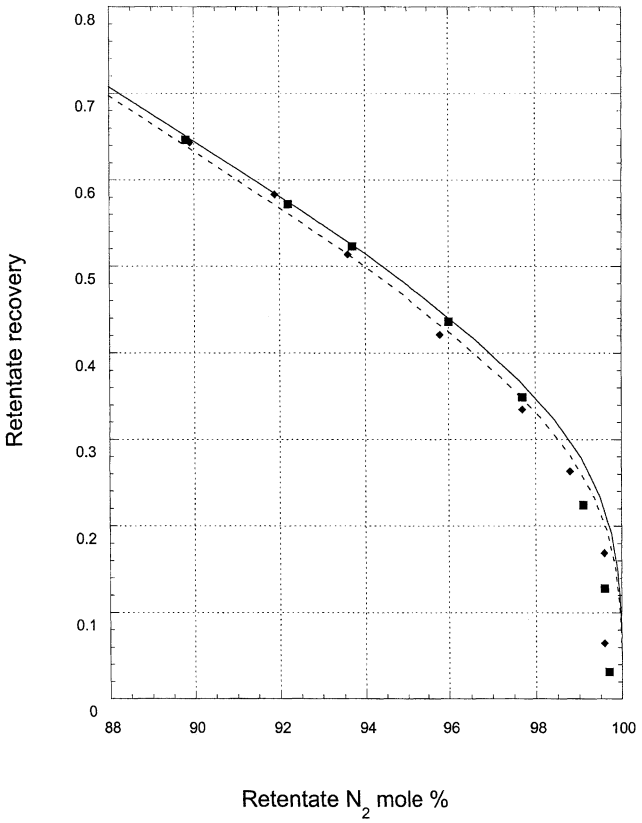

Figure 9. Experimental and theoretical performance for each module.

The lines in the figures are: solid line, theoretical results for module 1; short dash, theoretical results for module 2. The marks are: ■ experimental results for module 1; ◆ experimental results for module 2.

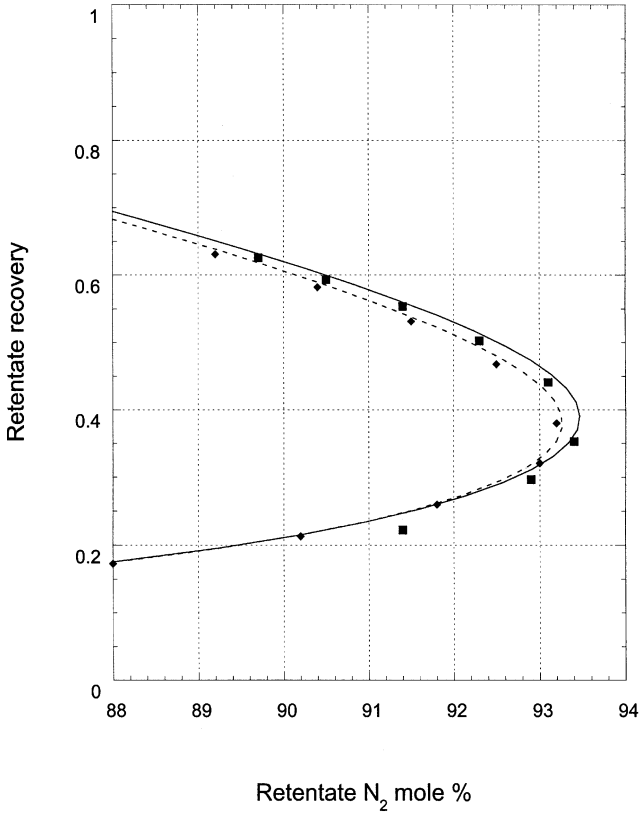

Figure 10. Experimental and theoretical performance for each module with the bypass tube.

The lines in the figures are: solid line, theoretical results for module 1; short dash, theoretical results for module 2. The marks are: ■ experimental results for module 1; ◆ experimental results for module 2.

is also shown. Module 1 performs slightly better than module 2. At higher recoveries, experimental results agree well with theoretical predictions. However, at low recoveries (or, equivalently, high nitrogen purities), significant performance deviations exist between theory and experiment. Moreover, experimental nitrogen purities in excess of 99.6% cannot be achieved. We believe the main reason for these deviations is variation in fiber properties, but other factors, such as shell flow maldistribution, may contribute. We did not pursue this issue further, because the deviations do not significantly affect performance predictions with the bypass tube as described next.

Figure 10 illustrates the dependence of performance on product purity for each module with the bypass tube. As in the absence of the bypass tube, module 1 performs slightly better than module 2. Predicted performance for each system is in excellent agreement with experiments. Particularly noteworthy is the ability to predict the maximum product purity of the systems; both cannot produce a purity of greater than $\sim 93.5\%$ nitrogen. This is consistent with prior work (Lemanski and Lipscomb, 2000).

Figure 11 illustrates the performance of the two-stage system with and without bypass tubes for each module. For comparison, the performance of the second module with bypass tube (taken from Figure 10) is also shown. Without the bypass tubes, experimental results and theoretical predictions are in good agreement at high recoveries. For lower recoveries (that is, higher product nitrogen purities), theoretical predictions deviate significantly from experiment; experimental performance is poorer than expected. This is similar to the results for each module in Figure 9, and we attribute the deviation to the same factors.

For the two-stage system with the bypass tube, agreement between theory and experiment is good over the entire composition range studied. As observed for a single stage, product nitrogen purity does not increase monotonically with decreasing recovery. Purity increases as recovery decreases to ~ 0.20, but then decreases as recovery decreases further. The two-stage system performs significantly better than a single stage with the bypass tubes. The maximum product nitrogen purity for the two-stage system is $\sim 98\%$ compared to $\sim 93.5\%$ for a single stage. Additionally, for a given product purity, the recovery of the two-stage system is higher than that of a single stage. The increase in recovery is especially dramatic at higher purities. We believe the ability to predict these striking changes in recovery and maximum product purity strongly supports the validity of the theoretical analysis since previous analyses of staging that neglect property variation would predict no change.

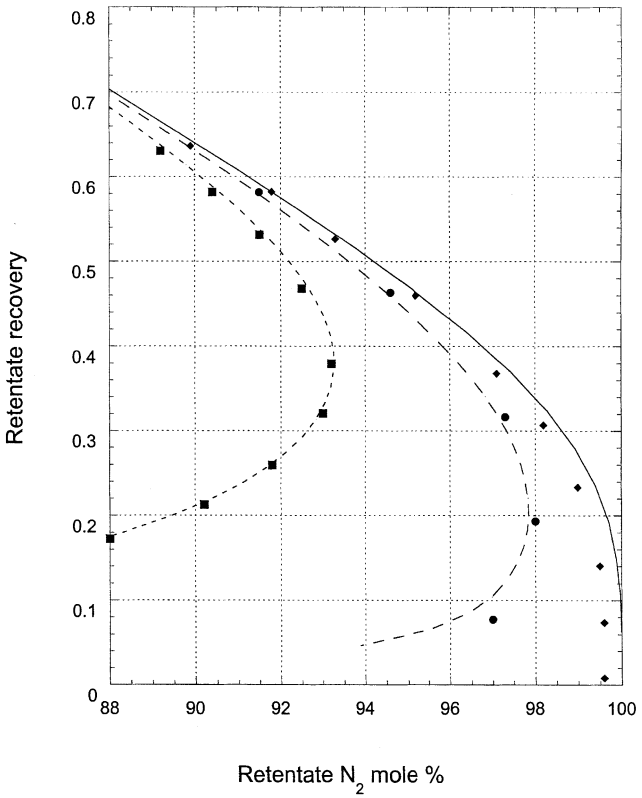

Figure 11. Experimental and theoretical performance for a two-stage system.

The lines in the figures are: solid line, theoretical results for the two-stage system with no bypass; long dash, theoretical results for the two-stage system with bypass; short dash, theoretical results for module 2 with bypass. The markers are: ♦ experimental data for two-stage system with no bypass; ● experimental data for two-stage system with bypass; ■ experimental data for module 2 with bypass.

Conclusions

An analysis of the effect of fiber property variation on the performance of a two-stage, hollow fiber membrane, gas separation system is presented. The analysis is based on mass and momentum balances and standard gas permeation expressions that incorporate the effects of Gaussian variations in ID, slow gas permeance, and selectivity.

Variation in any property is detrimental to performance. ID variations have the greatest effect for a given percent variation. Variations in permeance and selectivity lead to similar, but smaller, performance declines.

At high product purities, some fibers can stop producing product and consume a fraction of the product produced by other fibers. This phenomenon is predicted to occur only in the presence of ID and permeance variations.

Module staging can significantly improve performance in the presence of property variation. Staging can help reduce the extent to which complete permeation occurs and thereby increase purity and recovery over that achievable in a single stage. Permeate mixing also improves performance with ID and permeance variations. However, permeate mixing does not affect performance for selectivity variations.

Experimental results for a two-stage system designed to mimic permeance variations are in good agreement with theoretical predictions. Moreover, the results demonstrate that staging can dramatically improve performance over that achievable in a single stage in the presence of property variations.

This work provides a sound theoretical basis for the optimization of networks of gas separation modules in the presence of fiber variations. We anticipate the need to account for the effects of variations will be especially important at the higher purity limits of current commercial systems. Moreover, manufacturers now have a new tool for evaluating how tightly to control fiber properties. A manufacturer may forego expensive process improvements to reduce property variation if staging provides the same benefit.

Acknowledgment

The authors acknowledge partial support of this work by the National Science Foundation through grant CTS-9408414.

Notation

F = feed flow rate, $\text{mol}\cdot\text{s}^{-1}$
g = fiber property distribution function
ID = fiber inside diameter, m
J = dimensionless gas permeation rate
l = effective membrane thickness, m
L = total active fiber length, m
N^h = dimensionless group defined by Eq. 9
N^p = dimensionless group defined by Eq. 8
OD = fiber outer diameter, m
p = pressure, Pa
P = premeate flow rate, $\text{mol}\cdot\text{s}^{-1}$
Q = permeance, $\text{m}^3(\text{STP})/\text{m}^2\cdot\text{s}\cdot\text{Pa}$, ratio of intrinsic permeability to effective membrane thickness
R = retentate flow rate, $\text{mol}\cdot\text{s}^{-1}$
R_g = ideal gas constant, $\text{Pa}\cdot\text{m}^3\cdot\text{mol}^{-1}\cdot\text{K}^{-1}$
T = operation temperature, K
w_i = Gauss-Hermite quadrature weight points
x = fast gas mol fraction in retentate
y = fast gas mol fraction in permeate
z = dimensionless flow path length

Greek letters

α = permselectivity
γ = pressure ratio
Δ = change in pressure
θ = ratio of flow rate to feed flow rate
μ = retentate viscosity, $\text{Pa}\cdot\text{s}$
Π = ratio of actual retentate pressure to feed pressure
σ = standard deviation
ϕ = arbitrary fiber property

Subscripts

f = feed
max = maximum value
min = minimum value
P = permeate value
R = retentate value
S = system value
1 = first stage
2 = second stage
$-$ = average value

Superscripts

A = fast gas
B = slow gas

Literature Cited

Carnahan, B., H. A. Luther, and J. O. Wikes, *Applied Numerical Methods*, Krieger, Malabar, FL (1990).

Crowder, R. O., and E. L. Cussler, "Mass Transfer in Hollow Fiber Modules with Non-Uniform Hollow Fibers," *J. Memb. Sci.*, **134**, 235 (1997).

Elmore, S., and G. G. Lipscomb, "Analytical Approximations of the Effect of Fiber Size Distribution on the Performance of Hollow Fiber Membrane Separation Devices," *J. Memb. Sci.*, **98**, 49 (1995).

Kruelen, H., C. A. Smolders, G. F. Verteeg, and W. P. M. van Swaaij, "Microporous Hollow Fiber Membrane Modules as Gas-Liquid Contactors: 1. Physical Mass Transfer Processes," *J. Memb. Sci.*, **78**, 197 (1993).

Lemanski, J., B. Liu, and G. G. Lipscomb, "Effect of Fiber Variation on the Performance of Cross-Flow Hollow Fiber Gas Separation Modules," *J. Memb. Sci.*, **153**, 33 (1999).

Lemanski, J., and G. G. Lipscomb, "Effect of Fiber Variation on the Performance of Counter-Current Hollow Fiber Gas Separation Modules," *J. Memb. Sci.*, **167**, 241 (2000).

Lipscomb, G. G., "Design of Hollow Fiber Contactors for Membrane Gas Separations," *The 1996 Membrane Technology Reviews*, Business Communication Co., Norwalk, CT, p. 23 (1996).

MATLAB, The MathWorks Inc., Natick, MA (1995).

Qi, R., and M. A. Henson, "Optimal Design of Spiral-Wound Membrane Networks for Gas Separations," *J. Memb. Sci.*, **148**, 71 (1998).

Rautenbach, R., A. Struck, and M. F. M. Roks, "A Variation in Fiber Properties Affects the Performance of Defect-Free Hollow Fiber Membrane Modules for Air Separation," *J. Memb. Sci.*, **150**, 31 (1998).

Wickramasinghe, S. R., M. J. Semmens, and E. L. Cussler, "Mass Transfer in Various Hollow Fiber Geometries," *J. Memb. Sci.*, **69**, 235 (1985).

Manuscript received Sept. 29, 2000, and revision received Feb. 12, 2001.